Influence of dynamic topography on sea level and its rate of change

Clinton P. Conrad[1]* and Laurent Husson[2]

[1]DEPARTMENT OF GEOLOGY AND GEOPHYSICS, SCHOOL OF OCEAN AND EARTH SCIENCE AND TECHNOLOGY (SOEST), UNIVERSITY OF HAWAII, HONOLULU, HAWAII 96822, USA
[2]GÉOSCIENCES RENNES, UNIVERSITÉ RENNES 1, CENTRE NATIONAL DE LA RECHERCHE SCIENTIFIQUE (CNRS), RENNES 35042, FRANCE

ABSTRACT

Mantle flow likely supports up to 2 km of long-wavelength topographic relief over Earth's surface. Although the average of this dynamic support must be zero, a net deflection of the ocean basins can change their volume and induce sea-level change. By calculating dynamic topography using a global mantle flow model, we find that continents preferentially conceal depressed topography associated with mantle downwelling, leading to net seafloor uplift and ~90 ± 20 m of positive sea-level offset. Upwelling mantle flow is currently amplifying positive dynamic topography and causing up to 1.0 m/Ma of sea-level rise, depending on mantle viscosity. Continental motions across dynamic topography gradients also affect sea level, but uncertainty over the plate motion reference frame permits sea-level rise or fall by ±0.3 m/Ma, depending on net lithosphere rotation. During a complete Wilson cycle, sea level should fall during supercontinent stability and rise during periods of dispersal as mantle flow pushes continents down dynamic topography gradients toward areas of mantle downwelling. We estimate that a maximum of ~1 m/Ma of sea-level rise may have occurred during the most recent continental dispersal. Because this rate is comparable in magnitude to other primary sea-level change mechanisms, dynamic offset of sea level by mantle flow should be considered a potentially significant contributor to long-term sea-level change.

LITHOSPHERE; v. 1; no. 2; p. 110–120. doi: 10.1130/L32.1

INTRODUCTION

During the mid-Cretaceous, several continents experienced oceanic transgressions that produced inland seas; the Western Interior Seaway of North America is a good example (e.g., Bond, 1976). These transgressions have been generally attributed to elevated eustatic sea level during the Cretaceous, which must have dropped by ~200 m to explain the observed continental inundations (e.g., Haq et al., 1987). Sea-level drops of this amplitude can be attributed to a major decrease in ridge volume, caused by a sustained shortening of the mid-ocean-ridge system or a slowdown in seafloor spreading rates (e.g., Pitman, 1978; Kominz, 1984; Xu et al., 2006; Cogné et al., 2006; Müller et al., 2008). However, recent sequence stratigraphy performed on the Atlantic seaboard of North America has cast doubt on the eustasy paradigm by suggesting a much smaller Cretaceous sea-level drop of only ~70 m or less (Miller et al., 2005), which could have been accomplished by climatic changes alone.

Recently, the discrepancy between these various observations of sea-level change has been attributed to vertical motion of continental margins caused by the dynamics of convection in Earth's mantle (Moucha et al., 2008; Müller et al., 2008). In particular, the east coast of North America lies above the subducted Farallon slab, which subducted beneath the U.S. west coast prior to 30 Ma, and it is observed today as a seismically fast anomaly in the lower mantle beneath the U.S. east coast (Bunge and Grand, 2000). The descent of this cold, dense feature is thought to be driving downwelling viscous flow that pulls the western half of the North Atlantic seafloor downward by ~0.5 km with respect to the eastern half (Conrad et al., 2004). In fact, nonisostatic topographic relief up to ~2 km or more has been attributed to dynamic support from viscous mantle flow in modeling studies (e.g., Hager et al., 1985), and numerous topographic features such as backarc basins (Husson, 2006), the Western Interior Seaway (e.g., Mitrovica et al., 1989), or the plateaus of southern Africa (Lithgow-Bertelloni and Silver, 1998; Gurnis et al., 2000) have been shown to be dynamically supported. On the U.S. east coast, the westward motion of North America over the Farallon slab should have produced dynamic subsidence since at least the Eocene (Liu et al., 2008; Spasojeviç et al., 2008). Combined with a global fall in sea level, this downward motion of the coastline may explain the anomalously small sea-level change that Miller et al. (2005) observed for the U.S. east coast. In fact, coastlines around the world are likely in constant motion as a result of the dynamics of the mantle interior, which significantly complicates the interpretation of relative sea-level measurements worldwide (Moucha et al., 2008).

While dynamic topography may dramatically affect observations of sea level made on coastlines, it is also possible that dynamically supported deflections of ocean basin seafloor can lead to a net change in global eustatic sea level. For example, Gurnis (1990) suggested, using a simple two-dimensional (2-D) model, that faster plate motions and fatter ridges should also produce growing slab anomalies that increase the negative dynamic topography near convergent margins, leading to continental inundation (Gurnis, 1993). The effect of this dynamic topography is to diminish the sea-level rise associated with the ridge volume change. Husson and Conrad (2006), however, used simple boundary layer theory to show that if plate acceleration is facilitated by a change in mantle viscosity, the effect of dynamic topography on basin volume, and thus sea level, is diminished. Furthermore, they showed that a sustained increase in plate motions leads to thinner mantle slabs, a positive change in dynamic topography, and elevated sea level. Thus, changes in plate motion should lead to a net change in eustatic sea level, but the amplitude, and even the sign, of the response depends on the time scales and causes of the plate motion change.

*Corresponding author e-mail: clintc@hawaii.edu.

In practice, the mantle interior and surface plate motions are more complicated than suggested by either idealized 2-D modeling or boundary layer theory. Seismic tomography reveals complicated patterns of fast and slow velocity anomalies (e.g., Ritsema et al., 2004), some of which may be associated with slabs and upwelling flow, respectively. The dynamic topography produced by this flow should affect sea level (Fig. 1); for example, the depression of the western North Atlantic by the Farallon slab (Conrad et al., 2004) should increase the volume of the North Atlantic basin, and thus should lower sea level globally (Fig. 1, mode 1). Furthermore, continental regions move laterally over this time-varying dynamic topography field, variously exposing or concealing this deflected topography from the ocean basins, where it can affect sea level (Fig. 1, mode 2). To gain a full understanding of the ways in which mantle flow uplifts Earth's surface as a function of time, three-dimensional, time-dependent flow models are required in which dynamic topography is tracked temporally (e.g., Gurnis et al., 2000; Conrad and Gurnis, 2003). For example, Moucha et al. (2008) examined a full model for the past 30 Ma of global mantle flow and found that changes in dynamically supported seafloor topography caused eustatic sea level to rise ~100 m during this time period, or ~3 m/Ma.

In this study, we examine the ways in which the dynamics of viscous mantle flow affect average seafloor bathymetry and, thus, eustatic sea level. In particular, we consider the effects of mantle downwelling (driven by fast seismic anomalies, typically associated with slabs) and mantle upwelling (driven by slow seismic anomalies) separately. We also examine the relative importance of upper-mantle and lower-mantle flows, as well as the importance of mantle viscosity structure. Finally, we examine the relative contributions of time-varying dynamic topography (Fig. 1, mode 1) and continental motion (Fig. 1, mode 2) to the total net sea-level change. Because these two mechanisms are constantly operating together to affect sea-level change, it is difficult to extract their relative importance in a time-dependent dynamic model with plate motions (e.g., Moucha et al., 2008). However, we can constrain their relative importance by examining each effect separately and instantaneously. Therefore, we restrict our analysis to the present-day mantle flow field and its first time-derivative. Furthermore, the understanding gained from our analysis allows us to estimate the ways in which dynamic topography may affect sea level throughout a Wilson cycle (e.g., Wilson, 1966) of supercontinent aggregation and dispersal.

ESTIMATING DYNAMIC TOPOGRAPHY AND SEA-LEVEL OFFSET FROM GLOBAL MANTLE FLOW MODELS

To constrain the effect of dynamic topography on sea level, we first developed global mantle flow models that can be used to predict the time-dependent patterns of topography that are dynamically supported by the mantle's present-day flow field. To do this, we employed a spherical finite element code (CitComS [Zhong et al., 2000; Tan et al., 2006], accessed in January 2009 to obtain a version that includes recently added self-gravitation effects [Zhong et al., 2008]) to predict present-day mantle flow in a spherical Earth driven by the mantle's internal density heterogeneity. We used the S-wave seismic tomography model S20RTSb (Ritsema et al., 2004) to infer lateral variations of density within the mantle and employed a constant conversion factor of 0.15 g cm^{-3} km^{-1} s to convert seismic velocity anomaly to density anomaly. We chose this conversion factor because it is consistent with both laboratory data (e.g., Karato and Karki, 2001) and with previous studies (e.g., Conrad et al., 2007) (although this choice is accompanied by some uncertainty in both magnitude and potential depth-dependence). Also following previous work (e.g., Lithgow-Bertelloni and Silver, 1998; Conrad et al., 2007), we did not impose density anomalies above 300 km depth because seismically fast velocity anomalies associated with continental roots have been shown to correspond to neutrally buoyant

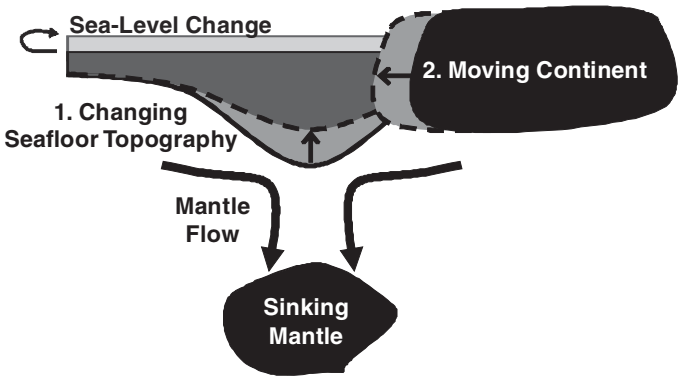

Figure 1. Two mechanisms by which dynamic topography can change sea level with time. Mode 1: Time-dependent mantle flow changes the pattern of seafloor dynamic topography. For the case shown, a mantle downwelling moves away from the surface, which causes the dynamic topography above the downwelling to become less depressed (e.g., Mitrovica et al., 1989), resulting in sea level rise. Mode 2: A continent moves laterally over a region of anomalously low topography. This moves the average dynamic deflection of the seafloor toward more positive values, which elevates sea level.

"tectosphere" (e.g., Jordan, 1975), which implies that a straightforward conversion between seismic velocity and density is not appropriate for the continental lithosphere. Similarly, slow velocity anomalies detected near the surface beneath ridges (e.g., Ritsema et al., 2004) may be associated with decompression melting of passively upwelling mantle rocks. These near-surface anomalies require a very different treatment than we have applied below 300 km (e.g., Hernlund et al., 2008).

We assume a reference viscosity structure equivalent to the one that Conrad et al. (2007) used to successfully predict seismically anisotropic fabric beneath the ocean basins. This structure is entirely radial and ignores lateral viscosity variations; it includes a low-viscosity asthenosphere (between 300 and 100 km depth) that is a factor of 10 less viscous than the upper mantle, and higher-viscosity lower mantle (below 670 km) and lithospheric (above 100 km) layers that are 50 and 30 times more viscous than the upper mantle, respectively. This reference viscosity structure is similar to the one used by Lithgow-Bertelloni and Richards (1998) to predict the shape of the geoid and plate motions. Although the magnitude of dynamic topography is not sensitive to the absolute value of mantle viscosity, but only to its radial (e.g., Hager, 1984) and lateral (Cadek and Fleitout, 2003) variations, the rate of change of dynamic topography, which we examine next, is directly dependent on this absolute value. Therefore, we initially assume an upper-mantle viscosity of 0.5×10^{21} Pa s, which is consistent with estimates constrained from postglacial rebound (e.g., Mitrovica, 1996), and equal to the value that provides the best fit to anisotropy observations in Conrad et al.'s (2007) flow models.

In fact, the reference flow model that we develop here is the same as the highest-resolution model used by Conrad et al. (2007) (with 105 km horizontal and 17 km vertical resolution in the upper half of the upper mantle, and 100 km vertical resolution in the lower mantle; lower-resolution calculations produce similar results), with one exception. Conrad et al. (2007) combined flow driven by mantle density heterogeneity beneath a rigid surface boundary condition with flow driven by surface velocity boundary conditions consistent with observed plate motions. Neither condition is consistent with the free-slip surface condition of Earth, but they are consistent with observed plate motions. Here, we use free-slip surface boundary conditions to predict dynamic topography, as others have done (e.g., Zhong and Davies, 1999; Lithgow-Bertelloni and Richards, 1998), because

Thoraval and Richards (1997) found that this boundary condition provides a better fit to the geoid than rigid or plate motion boundary conditions.

We calculated dynamic topography globally by computing the radial traction, σ_{zz}, that mantle flow exerts on the free-slip surface, perturbed to include self-gravitation effects using Zhong et al.'s (2008) implementation in CitcomS. For Earth's free surface, this perturbed radial stress is compensated by the mass anomaly associated with topographic deflection of the surface equal to $h = \sigma_{zz}/\Delta\rho g$, where g is the acceleration due to gravity and $\Delta\rho$ is the density contrast between seawater and mantle rocks, which we take to be 2310 kg/m^3. Note that continental areas feature a density contrast of 3340 kg/m^3 because subaerial topographic deflections are compensated by air rather than seawater. This reduces the amplitude of dynamically supported topography in continental areas, but it does not affect our estimates of seawater reservoir sizes unless topography crosses sea level during its deflection, which is a second-order effect that we will ignore here.

We measure the offset of average sea level caused by dynamic deflections of the seafloor relative to a (theoretical) static Earth with no dynamic topography. To do this, we considered that sea level is a geopotential surface known as the geoid, which we also computed using the self-gravitation implementation in CitcomS. Although Earth's internal density heterogeneity and dynamically deflected surfaces do produce geoid topography at a range of scales (e.g., Hager, 1984; Hager et al., 1985; Lithgow-Bertelloni and Richards, 1998), this sea-surface topography does not deflect average sea level because the geoid reference level is an arbitrary surface. A net deflection of the seafloor by dynamic topography, however, will cause a corresponding offset of sea level if the volume of seawater is constant (e.g., Moucha et al., 2008). To measure this offset, we express dynamic topography relative to a spherical surface centered on Earth's center of mass (e.g., Paulson et al., 2005). Thus, we remove the degree-one component of the geoid, which expresses offset of center of mass in the calculation coordinates, from the predicted dynamic topography. Note that the degree-one component of the resulting dynamic topography need not be zero if there is a net deflection of Earth's surface in one direction that is caused by degree-one density heterogeneity within Earth's interior. We ignore the degree-zero component of dynamic topography because its choice is arbitrary. The resulting dynamic topography (Fig. 2), which we compute as the sum of spectral degrees 1–20, is thus the net surface deflection that is dynamically supported by density heterogeneity in Earth's mantle. The associated geoid variations are generally anticorrelated to dynamic topography and are an order of magnitude smaller (e.g., Hager, 1984). As described already, geoid variations do not produce a net eustatic sea-level offset, but they may affect local measurements of sea level relative to the continents, which themselves may be experiencing time-dependent dynamic deflections (Moucha et al., 2008).

OFFSET OF SEA LEVEL BY DYNAMIC TOPOGRAPHY

Surface deflections associated with the previously described flow models show that Earth's surface presents positive dynamic topography above the two "superplumes" beneath southern Africa and the southern Pacific and negative dynamic topography near the major subduction zones of South America and Southeast Asia (Fig. 2A). Although some studies have suggested smaller magnitudes of topography than we estimate here (Colin and Fleitout, 1990; Le Stunff and Ricard, 1997), several recent studies have constrained similar or even larger amplitudes (e.g., Lithgow-Bertelloni and Gurnis, 1997; Moucha et al., 2008). Furthermore, our predictions are consistent with geologic observations of up to ~1 km uplift of southern Africa (Lithgow-Bertelloni and Silver, 1998; Gurnis et al., 2000) and up to ~0.5 km topography differential across the North Atlantic (Conrad et al., 2004).

If we integrate the mantle tractions that support dynamic topography over the entire surface of the globe, we find that the total of this dynamic support integrates to zero. This is an expected result of mantle circulation: every upwelling or downwelling that dynamically supports surface topography must be balanced by return flow (downwelling or upwelling, respectively) that supports opposing topography somewhere else on the globe. Thus, if oceans covered the entire globe, the net effect of dynamic topography on sea level would be zero. However, because continents cover nearly one third of the globe, a net deflection of continental areas by mantle flow will be balanced by an opposing net deflection of oceanic areas, leading to a net offset of sea level. This is exactly what we find: our model predicts an average dynamic uplift of the seafloor (Fig. 2A) by 132 m, while continental areas are depressed by an average of 295 m. Although compensation by air reduces continental dynamic topography by 70% compared to water-covered areas, the average continental deflection is larger than it is for ocean basins because continental area is 2.24 times smaller than ocean area. The continental deflection is negative because subduction tends to put slabs, and thus mantle downwelling, beneath continents (e.g., Asia, Australia, and South America in Fig. 2A). Because the changes to the water column above vertically deflected seafloor will be isostatically compensated, our estimate of 132 m of dynamic seafloor uplift actually elevates sea level by only 92 m (70%; Pitman, 1978; Husson and Conrad, 2006; Müller et al., 2008).

We performed a similar analysis to approximately constrain the mantle sources of the various features in the net dynamic topography field (Fig. 2A). To start, we calculated the dynamic topography produced by flow driven only by negative (Fig. 2B) and positive (Fig. 2C) density heterogeneities in the upper mantle, which generate active upwelling and downwelling, respectively. We find that these flow fields produce similar patterns of dynamic seafloor topography and offset sea level approximately equally (23 and 22 m, respectively), despite very different driving mechanisms. Active upwelling generates positive topography near Iceland, in the southern and northeast Pacific basin, and east of Africa, and passive return flow depresses Earth's surface elsewhere (Fig. 2B). Active downwelling is associated primarily with slabs in the western Pacific and South America, and it depresses the surface above them, while passive return flow uplifts the surface elsewhere (Fig. 2C). We observe similar patterns and amplitudes of topography supported by active upwelling and active downwelling in the lower mantle (Figs. 2D and 2E, which yield 25 and 23 m of sea-level offset, respectively). The lower-mantle response, however, is typically confined to longer wavelengths and features a stronger influence of the African superplume (Fig. 3D) and Farallon slab (Fig. 2E) than do the upper-mantle flows. The similar pattern observed for upwelling-driven (Figs. 2B and 2D) and downwelling-driven (Figs. 2C and 2E) flows indicates that areas of upwelling typically occur in the location of return flow from areas of downwelling, and vice versa. These four components of the flow field (Figs. 2B–2E) sum to the total topography (Fig. 2A) and contribute to positive sea-level offset approximately equally.

TIME-DEPENDENCE OF DYNAMIC TOPOGRAPHY AND SEA-LEVEL CHANGE

Because the patterns and amplitudes of dynamic topography change with time, the net offset of sea level by dynamic topography should change as well, resulting in a net sea-level rise or fall (Fig. 1, mode 1). To estimate the rate at which changing dynamic topography affects sea-level change, we used the previous flow model to advect the mantle's density heterogeneity field forward in time. As mantle density heterogeneity evolves with time, the mantle flow field does as well, which changes the dynamic topography field. We measured the rate of change of dynamic

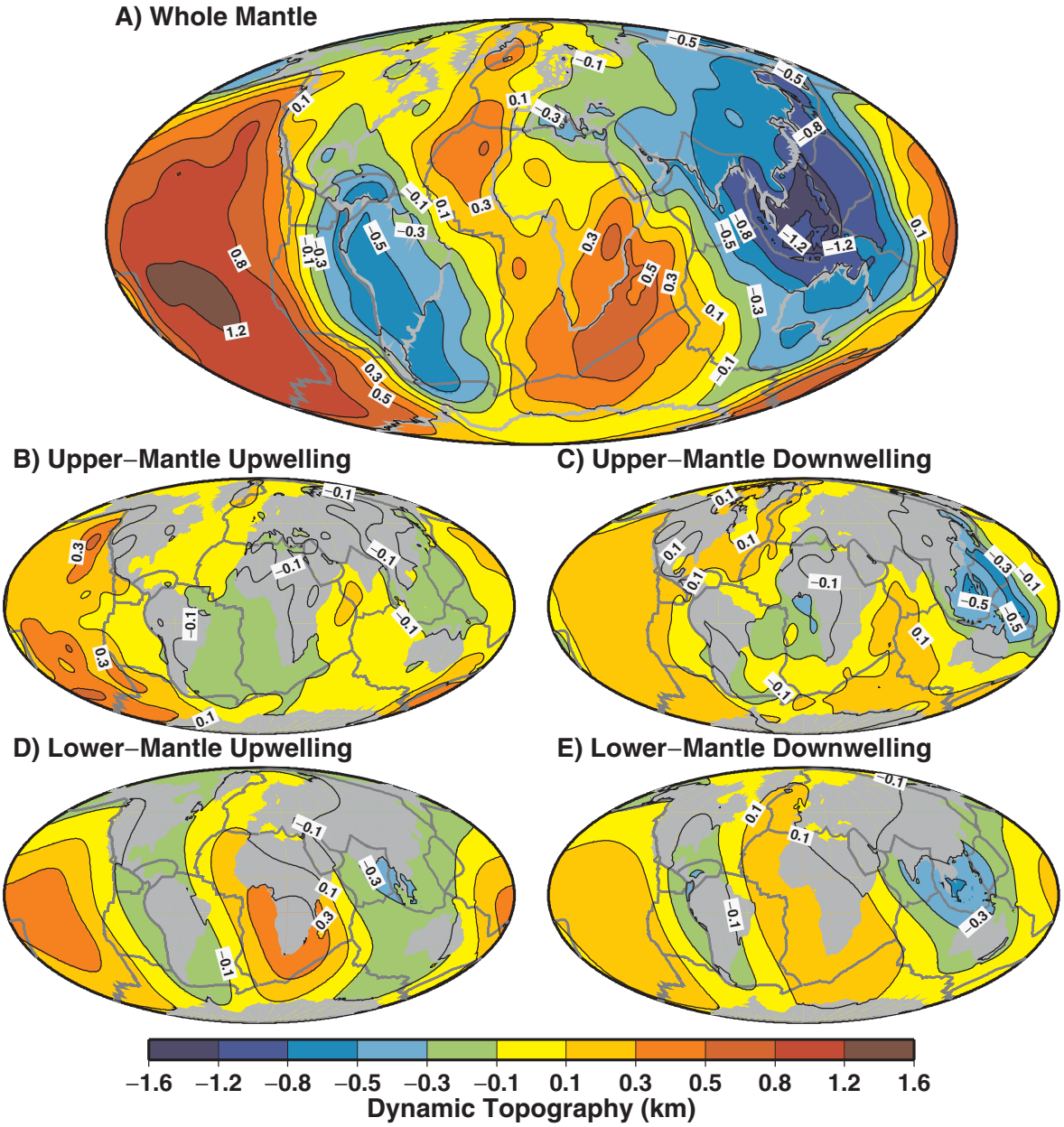

Figure 2. Dynamic topography determined by calculating mantle flow using density heterogeneity in (A) the whole mantle, and separated into portions driven by (B) negative density and (C) positive density anomalies in the upper mantle, and (D) negative density and (E) positive density anomalies in the lower mantle. Thus, parts B and D show topography associated with active upwelling flow, while C and E are driven by downwelling flow.

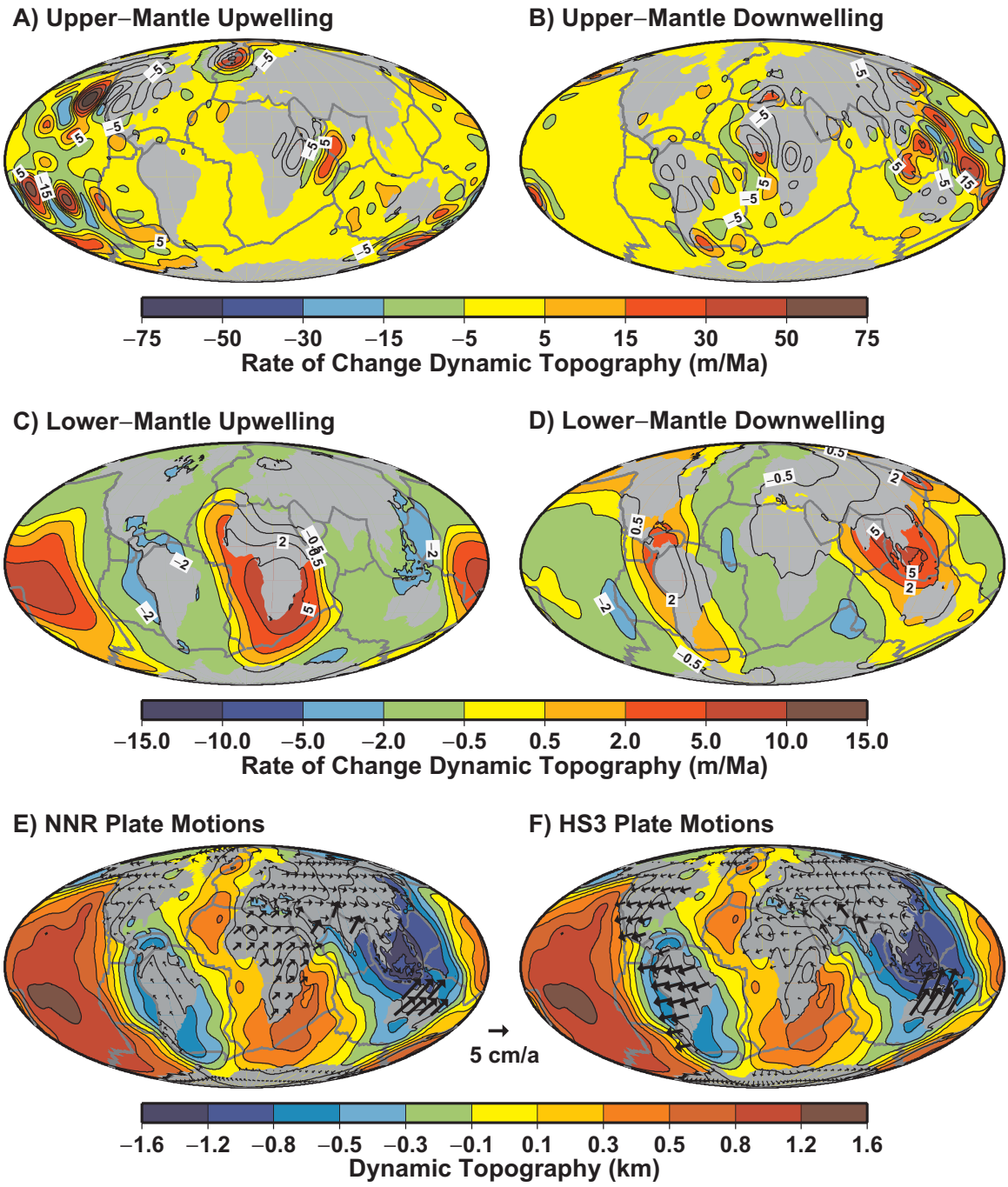

Figure 3. Rate of change of dynamic topography (e.g., Fig. 1, mode 1) determined from time-dependent flow models for (A–D) subsets of the flow field as broken down in Figures 2B–2E. Sea-level change is also caused by continental motions over the dynamic topography field (e.g., Fig. 1, mode 2), as shown here for global mantle flow (from Fig. 2A) and plate motions in the (E) no-net rotation (NNR) (De Mets et al., 1994) and (F) HS3 (Gripp and Gordon, 2002) reference frames.

topography for both upwelling- and downwelling-driven flows in both the upper and lower mantles (Figs. 3A–3D). For the upper-mantle flows, we compared the dynamic topography at the beginning of the calculation and again at 1.0 Ma, because this time interval was long enough for an observable change in dynamic topography to occur but short enough that the mantle's behavior is still approximately linear. From these two maps, we computed their time variation and obtained maps of the rate of change of dynamic topography driven by upper-mantle upwelling and downwelling (Figs. 3A and 3B). Because the higher viscosity of the lower mantle yields a slower evolution of the mantle flow field, we found that 2.0 Ma were necessary to resolve the time variation of dynamic topography induced by lower-mantle upwelling and downwelling (Figs. 3C and 3D).

By comparing maps of dynamic topography (Figs. 2B–2E) with its time variation (Figs. 3A–3D), we can infer the way in which dynamic topography is changing with time, as well as the implications for sea-level change. In general, we find that positive surface deflections above upwellings (Figs. 2B and 2D) tend to become reinforced (Figs. 3A and 3C), while negative deflections above areas of downwelling (Figs. 2C and 2E) tend to become diminished (Figs. 3B and 3D). For example, dynamic topography above the lower-mantle African and South Pacific superplumes (Fig. 2D) is growing (Fig. 3C). This is because the low-density mantle anomalies that support this elevated topography are moving closer to the surface, where they can produce additional surface uplift. By contrast, the negative topography above the western Pacific and South American slabs (Fig. 2E) is becoming less negative, as shown by the positive uplift in these regions (Fig. 3D). This occurs because these lower-mantle slabs are sinking away from the surface, which diminishes their ability to induce topography there. Upper-mantle flows show similar patterns of positive uplift above both active upwelling (e.g., the growing uplift in Iceland, and the northeastern and southern Pacific in Fig. 3A) and active downwelling regions (e.g., the upwelling above western Pacific slabs in Fig. 3B), although the shorter-wavelength nature of upper-mantle flows tends to locate return flow, and its associated depressing topography, closer to locations of growing topography.

Many of the lower-mantle patterns in Figures 3C and 3D are consistent with trends found in previous studies. For example, ongoing uplift of Africa was predicted by Gurnis et al. (2000), as was uplift of much of the Pacific by Moucha et al. (2008) during the past 30 Ma. We observe both trends here associated with the upward motion of lower-mantle upwelling (Fig. 3C). Liu et al. (2008) showed that the amplitude of subsidence of North America has been decreasing as the Farallon slab descends; this result was predicted by Mitrovica et al. (1989) and is observed here (Fig. 3D). However, our prediction of continuing uplift of South America and the western Pacific (Fig. 3D) is not supported by either time-dependent flow models or geologic evidence. Instead, these trends are caused by the descent of lower-mantle slabs away from the 670 km interface without the ongoing resupply of slab material that we would expect from continuous subduction at the surface. Unlike Farallon subduction beneath North America, both the western Pacific and South America have seen continuous subduction at least through the Cenozoic (Sdrolias and Müller, 2006), so surface upwelling in these areas (Fig. 3D) is probably not representative of the long-term dynamics of these areas. At best, uplift above these continuously subducting slabs may be representative of an end member case in which slabs have stalled at the 670 km discontinuity while their lower-mantle portions fall away, as may be occurring in Tonga (van der Hilst, 1995). However, because slabs do not appear to be stalling at 670 km depth everywhere, uplift above subduction zones shown in Figure 3D and the subsidence away from them associated with return flow are almost certainly overestimated. Similarly, uplift above upper-mantle slabs falling away from 300 km depth (Fig. 3B) is also probably overestimated.

In practice, the time-dependence of dynamic uplift or subsidence above active subduction zones is difficult to constrain because a full treatment of time-dependent subduction dynamics is required; this has not yet been fully realized for a global model. Because of this, we will only consider time-dependence associated with upwelling flow (Figs. 3A and 3C) in the subsequent analysis, but we anticipate that downwelling flow could also induce time-dependence with magnitudes up to those estimated here (Figs. 3B and 3D), but with potentially an opposite sign if the time-dependence of subduction is currently placing material into the shallow mantle faster than it is falling away. In principle, upwelling flow calculations have potentially the same problems as downwelling flows models, but in reverse: low-density upwelling material also cannot be removed from our model as it rises toward the surface, and thus will also always produce surface uplift. However, with the exception of Iceland (Fig. 3A), most of the uplifting areas (Figs. 3A and 3C) do not occur near ridges, so there is no obvious sink for upwelling material analogous to the sources of downwelling material (subduction zones). Note that the lack of accurate sources and sinks for mantle density heterogeneity in time-dependent flow models has been noted before (e.g., Conrad and Gurnis, 2003), and it should influence other studies that advect mantle density heterogeneity (e.g., Moucha et al., 2008).

With these caveats in mind, we measured the average rate of change of dynamic topography (Fig. 3) over the oceanic areas to see if the estimated 92 m of dynamically supported sea level is changing with time. We find that active upwelling in the upper and lower mantles increases the average seafloor dynamic topography at rates of 0.42 and 0.20 m/Ma, respectively, producing 0.30 and 0.14 m/Ma of sea-level rise when isostatically compensated. The positive sign in this case occurs because upwelling-induced uplift, which is amplifying as discussed already, preferentially occurs in oceanic areas. By contrast, downwelling-induced negative topography, which is uplifting in our model, tends to occur beneath continental areas, leading to net subsidence of oceanic areas. As a result, active downwelling in the upper and lower mantles leads to 0.21 and 0.22 m/Ma of sea-level drop in our models, respectively. Taking only the upwelling components for the reasons described already, we estimate that the time-dependence of dynamic topography may cause up to 0.44 m/Ma of sea-level rise. The uncertainty in this estimate, however, is large because we do not know even the sign of the influence of downwelling flow. Our models suggest that at most 0.22 m/Ma of sea-level drop is associated with areas of downwelling in the lower mantle, but only if lower-mantle slabs are not being replenished by subduction. Using this value for the maximum amplitude of uncertainty (and ignoring the contribution from upper-mantle slabs, since we can be sure that they are being replaced by subduction), we estimate that 0.44 ± 0.22 m/Ma of sea-level rise is currently associated with time-dependent mantle flow.

UNCERTAINTY IN ESTIMATES OF SEA-LEVEL OFFSET AND RATE OF CHANGE

The amplitude of dynamic topography (Fig. 2) scales linearly with the velocity to density scaling factor, which is assumed to be 0.15 g cm^{-3} km^{-1} s here (this approximately corresponds to $\partial \ln[\rho]/\partial \ln[v_s] \sim 0.2$ in the terminology of Karato and Karki [2001]). Because mantle flow velocities also scale linearly with this scaling factor, the rate of change of dynamic topography scales with its square. Karato and Karki (2001) suggested that the uncertainty in $\partial \ln(\rho)/\partial \ln(v_s)$ may be on the order of about ±50% and may vary with depth, although significant deviation from our choice will cause predictions of dynamic topography (Fig. 2) to violate geologic constraints on its magnitude (e.g., Africa—Lithgow-Bertelloni and Silver, 1998; North Atlantic—Conrad et al., 2004). This factor may also be affected by

chemical heterogeneity, especially for low-velocity anomalies in the lower mantle (e.g., Masters et al., 2000). Thus, we acknowledge the important influence of the velocity to density scaling factor on our results, but we will use uncertainty in our viscosity model, which is also large, to evaluate uncertainty in our estimates of dynamic offset of sea-level offset, and its rate of change.

As described herein, the rate of change of dynamic topography scales inversely with the absolute mantle viscosity; thus, rates of sea-level change may be higher than those reported here if upper-mantle viscosity is larger than the value of 0.5×10^{21} Pa s that is assumed here. Although this viscosity value falls within the range of upper-mantle viscosities constrained by Mitrovica (1996) using postglacial rebound ($0.3–0.6 \times 10^{21}$ Pa s), these data may not adequately constrain viscosities for oceanic areas (Paulson et al., 2005), where a significantly weaker upper mantle may be possible (Paulson et al., 2007). Thus, uncertainty in the absolute value of mantle viscosity may induce up to a factor of two uncertainty in the rate of sea-level rise (Fig. 4). Lateral viscosity variations may introduce another source of uncertainty; while such variations in the mantle interior probably only exert a small influence on dynamic topography (Moucha et al., 2007), the effect of lithospheric variations (e.g., plate boundary or slab rheology) can be large, particularly for slab-induced downwelling flow (Zhong and Davies, 1999).

Because both dynamic topography and the geoid are sensitive to the mantle's radial viscosity structure (e.g., Hager, 1984; Lithgow-Bertelloni and Richards, 1998), we vary the viscosity of the lower mantle relative to that of the upper mantle to determine the range of possible variations in the dynamically supported sea-level offset (Fig. 5A) and its rate of change (Fig. 5B). (We determined in tests that the lower-mantle viscosity generally has a larger influence on these parameters than does the viscosity of the asthenospheric or lithospheric layers.) We find that the sea-level offset decreases with increasing lower-mantle viscosity (Fig. 5A) because density heterogeneity is increasingly compensated at the core-mantle boundary, rather than by surface deflections (Hager, 1984). For a range of lower-mantle viscosities between 30 and 100 times that of the upper mantle, we find that the sea-level offset ranges from 69 to 109 m (Fig. 5A). The sea-level rate of change (Fig. 5B) similarly exhibits a dependence on viscosity structure, and rates of change typically increase as lower-mantle viscosity decreases because of larger amplitude offsets (Fig. 5A) and faster rates of flow. The contributions from upper- and lower-mantle upwellings, for example, may be as large as 0.32 and 0.26 m/Ma for a viscosity contrast of 30 between the upper and lower mantles (Fig. 5B). These rates may be even larger if accompanied by a smaller absolute mantle viscosity (Fig. 4), but they may be close to zero for a higher lower-mantle (Fig. 5B) or absolute mantle viscosity (Fig. 4).

Taking all of these uncertainties into account, and considering that poor constraints on the effects of downwelling introduce additional uncertainty, we infer that sea level is currently positively offset by ~90 ± 20 m, and that the rate of change of this offset is highly uncertain but probably positive at the present time. Considering (1) that the range of lower-mantle viscosities allow upwelling flow to induce sea-level rise at up to 0.5 m/Ma (Fig. 5B), (2) that the uncertainty in the absolute viscosity permits a factor of ~2 variation, and (3) that mantle downwelling may cause sea level to drop (Fig. 5B), we constrain the rate of sea-level rise to rates of ~0.5 ± 0.5 m/Ma.

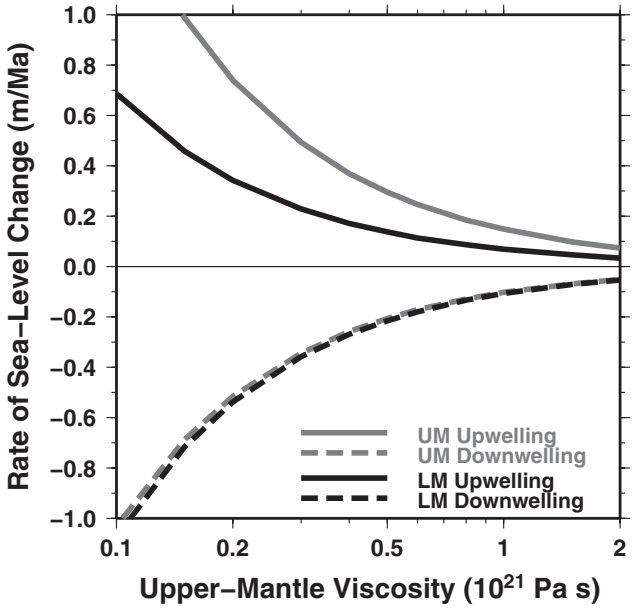

Figure 4. Rate of change of sea level caused by the time-dependence of dynamic topography as a function of the absolute value of upper-mantle viscosity. Calculations for dynamic topography driven by active upwelling and downwelling flow (solid and dashed lines), broken into upper-mantle (UM and lower-mantle (LM) components (gray and black lines), as in Figures 3A–3D, are shown separately.

CONTINENTAL MOTIONS AND SEA-LEVEL CHANGE

The horizontal motion of continents over dynamic topography can also lead to changes in sea level (Fig. 1, mode 2). To estimate the magnitude of this effect, we used observed present-day plate motions to advance the locations of the continents, as expressed on a 0.5 by 0.5 degree grid, forward in time by 5 Ma (significantly shorter time intervals do not allow for sufficient continental motion for differences in the continental masking of dynamic topography to be properly resolved) over the static dynamic topography field (Figs. 3E and 3F). Initially, we applied the NUVEL-1A model for present-day plate motions (DeMets et al., 1994) in the no-net rotation (NNR) reference frame. We find that the motion of continents over our reference model for dynamic topography (Fig. 3E) on average tends to cover up negative topography and expose positive topography, causing sea-level rise at a rate of 0.24 m/Ma. This trend is primarily caused by the motion of Asia and Australia toward the negative topography of the western Pacific (Fig. 3E). In this case, the predicted rate of sea-level change depends on rates of continental motion and not viscosity structure (at least not directly; rates of plate motion are ultimately dependent on mantle viscosity). Therefore, our constraints on the total sea-level offset (Fig. 5A) also apply to the continental motion over the dynamic topography that produces this offset. The resulting constraint (Fig. 5C) allows sea-level rise between 0.15 and 0.29 m/Ma.

Because patterns of dynamic topography are generated from depth, sea-level changes caused by motion of the continents over dynamic topography depend directly on the net rotation of the lithosphere relative to the deep mantle. Recently, the net lithosphere rotation has been a topic of some debate (e.g., Becker, 2006, 2008; Torsvik et al., 2008); most hotspot-based reference frames detect a present-day net westward motion of the lithosphere with poles of rotation clustered in the southern Indian Ocean (Becker, 2006). The amplitude of this net rotation, however, is much more variable and ranges from no-net rotation (NNR) (DeMets et al., 1994) to a maximum of 0.436°/Ma (for a maximum of 5 cm/a of westward motion) for the "HS3" Pacific hotspot model of Gripp and Gordon (2002); amplitudes for other studies fall somewhere between

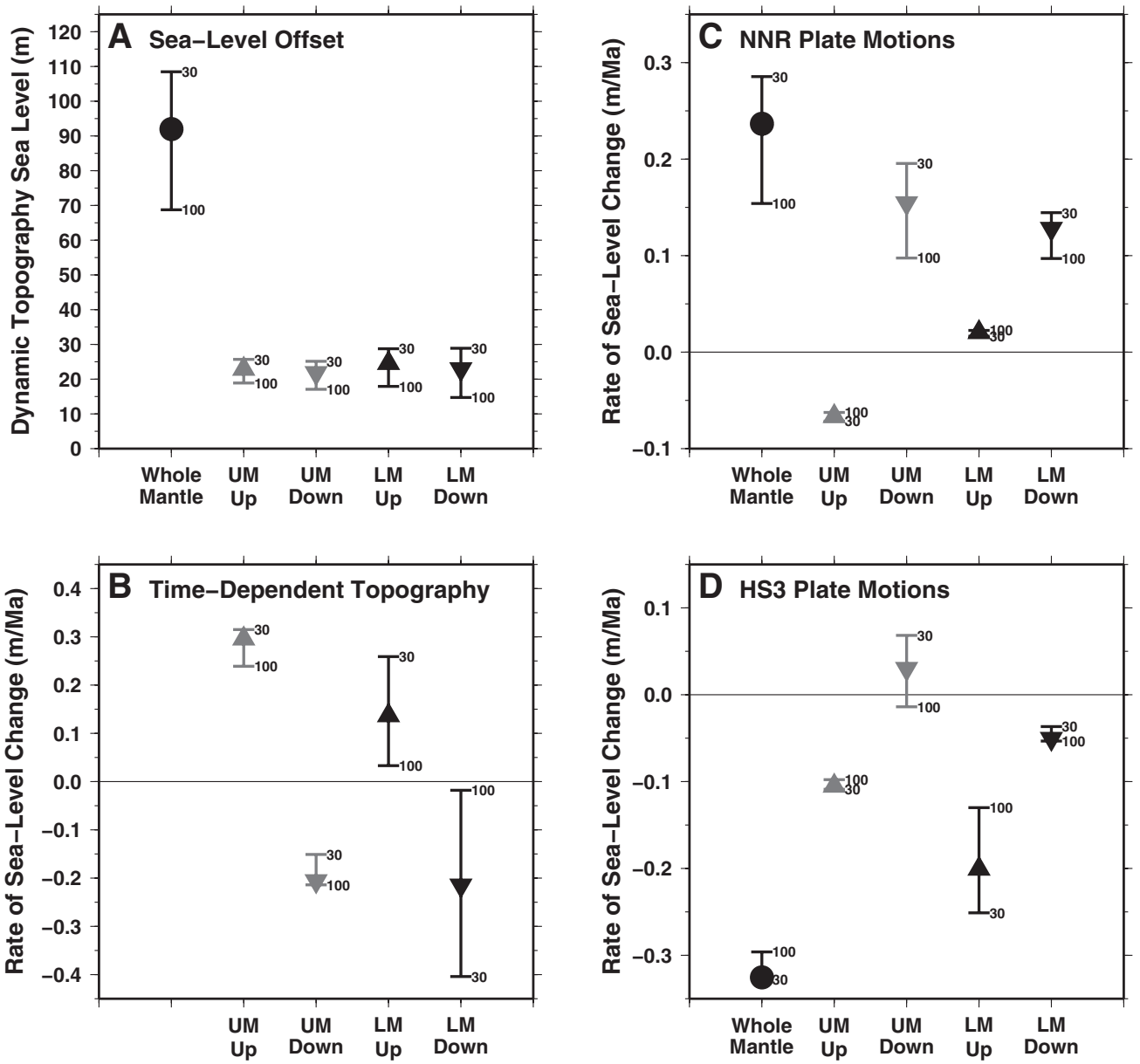

Figure 5. The effect of the lower-mantle viscosity on (A) the net present-day sea-level offset caused by dynamic topography, and the rate of change of this offset caused by either (B) the time-dependence of mantle flow (Fig. 1, mode 1) or continental motion (Fig. 1, mode 2) in the (C) no-net rotation (NNR) (De Mets et al., 1994) and (D) HS3 (Gripp and Gordon, 2002) reference frames. Flow is separated into four components as in Figures 2–4: upwelling (upward triangle) and downwelling (downward triangle) flows in the upper (gray) and lower (black) mantles. Solid dots show results for whole mantle flow, but the time-dependent component of this flow is not calculated in B because differing time scales control the upper-mantle (UM) and lower-mantle (LM) components (see text). Symbols show the results of calculations using lower-mantle viscosity that is 50 times that of the upper mantle (base model), while brackets show a range of this ratio varying from 30 to 100, as indicated.

these two extremes. Becker (2008) constrained a net rotation of ~50% of the amount implied by the HS3 model using anisotropy observations. To test the effect of net rotation on sea-level change rates, we added net rotation consistent with the end-member HS3 model (Gripp and Gordon, 2002) to the NNR plate motions. The introduction of this net rotation adds a westward drift to the continental motions (Fig. 3F), causes Eurasia to uncover negative dynamic topography in the western Pacific, and causes Africa and North America to cover positive dynamic topography in the Atlantic and Pacific basins, respectively. These changes are opposite to those produced by the NNR model, and they tend to lower sea level at a rate of 0.33 m/Ma with a small uncertainty (Fig. 5D).

Because dynamic topography caused by areas of upwelling and downwelling in the upper and lower mantles exhibits different spatial patterns (Figs. 2B–2E) than the dynamic topography of these fields combined (Fig. 2A), continental motion over these different topography fields produces a variety of effects on sea level. For example, sea-level rise produced by NNR motions is primarily associated with downwelling flow (Fig. 5C), while sea-level drop associated with HS3 motions is primarily associated

with upwelling flow (Fig. 5D). Altogether, we find that the net rotation of the lithosphere has a strong effect on sea-level change with time, and it can cause sea-level change ranging from sea-level rise at ~0.3 m/Ma for NNR to sea-level fall at ~0.3 m/Ma for HS3. As most constraints on net rotation fall somewhere between NNR and HS3 (e.g., Becker, 2006, 2008), sea-level change caused by continental motion should also fall between these extremes, and it should be nearly zero if Becker's (2008) estimate of 50% of the HS3 net rotation is correct. It is important to note that these results are for end member cases in which continents move over dynamic topography without regard to the mantle flow source of that topography. In fact, continental motions should be coupled to mantle flow, and thus should be correlated to dynamic topography, as we discuss next.

DISCUSSION: DYNAMIC OFFSET OF SEA LEVEL DURING A WILSON CYCLE

We can make inferences about the long-term effects of dynamic topography on sea level by interpreting the patterns predicted for the present day (e.g., Figs. 2–3) within the context of mantle evolution during a Wilson cycle of supercontinent aggregation and dispersal (e.g., Wilson, 1966; Phillips and Bunge, 2005; Zhong et al., 2007). We start by considering the lower-mantle flow field, which features basin-scale flow patterns that should evolve along with supercontinent aggregation and dispersal events (Collins, 2003). We have found that upwelling-dominated dynamic topography is currently amplifying at rates of 5–10 m/Ma (Fig. 3C). At these rates, the current ~500 m amplitude of the associated dynamic topography (Fig. 2D) could have grown entirely during the most recent continental dispersal event that began ~180 Ma ago with the opening of the Atlantic basin. Several authors that have studied the time-dependent evolution of lower-mantle structures (e.g., Conrad and Gurnis, 2003; Müller et al., 2008; Spasojeviç et al., 2008) have found that these structures develop over time scales on the order of 100 Ma because the high viscosity of the lower mantle produces sluggish flow. Therefore, it does not seem unreasonable that the lower-mantle component of our estimated sea-level change, up to ~0.25 m/Ma (Fig. 5B), should be maintained for a large fraction of the current continental dispersal event. Upper-mantle flow also produces long-wavelength topography (Figs. 2B–2C), but its time-dependence exhibits shorter wavelengths (Figs. 3A–3B). However, because the processes that control the evolution of upper-mantle density heterogeneity (e.g., superplume rise and seafloor aging) are also likely to develop on ~100 Ma time scales, we speculate that the upper-mantle contribution to dynamic offset of sea level may also evolve at time scales comparable to those of the lower mantle, and with similar magnitudes of up to ~0.3 m/Ma (Fig. 5B).

Since the long-wavelength patterns of dynamic topography are correlated with patterns of mantle flow, the motion of the continents should also be correlated with that flow, at least for long (plate-scale) wavelengths. For example, Bokelmann (2002) suggested that the North American plate has been decelerating as the cratonic root of North America becomes positioned above the center of the Farallon slab downwelling. Similarly, South America's motion may already be tied to the downwelling associated with the sinking Nazca slab (Fig. 2E). This motion of continents toward areas of downwelling occurs because upper-mantle flow, which typically moves from areas of upwelling toward downwelling, couples most strongly to the deep cratonic roots (Conrad and Lithgow-Bertelloni, 2006), pushing cratons away from areas of upwelling and toward areas of downwelling. In this view, cratons tend to move down gradients in dynamic topography; this process has been confirmed by evidence of net subsidence of continental interiors (Heine et al., 2008). This is the general pattern that is predicted for plate motions in the NNR reference frame (Fig. 3E), in which India, Eurasia, and Australia are moving toward the areas of downwelling in the western Pacific, Africa is moving away from the African upwelling, and North and South America are nearly stationary. Thus, the 0.25 m/Ma of sea-level rise associated with continental motion in the NNR frame (Fig. 5C) may apply for long-term sea-level change associated with continental motions during periods of continental dispersal, despite indications that a combination of the NNR and HS3 frames may be more appropriate for the present day (e.g., Becker, 2008). It is important to remember, however, that plates motions are controlled by a variety of factors, such as slab pull (e.g., Collins, 2003) or stress transfer across plates and upper mantle (e.g., Husson et al., 2008) that can generate continental motion up dynamic topography gradients (e.g., motion of South America or Eurasia in the HS3 model; Fig. 3F).

Because mantle upwelling is expected beneath a supercontinent during the dispersal phase of the Wilson cycle (e.g., Gurnis, 1988; Lowman and Jarvis, 1999), we expect that, on average, continents should be moving away from uplifted dynamic topography during dispersal, and later toward regions of low dynamic topography during reaggregation. Both phases involve continental motion down topography gradients, which should produce sea-level rise. We thus expect a corresponding sea-level drop during the supercontinent phase of the Wilson cycle, which can be ~150 Ma long (e.g., Hoffman, 1991). If supercontinent breakup occurs because of mantle upwelling (Gurnis, 1988; Lowman and Jarvis, 1999), then the downwelling that originally aggregated the supercontinent (note that subduction, and thus downwelling, is necessary for ocean basin closure) must develop into an upwelling. Considering that the net stress that the mantle exerts on the surface must always integrate to zero, a net uplift of the continental side of Earth during the lifetime of a supercontinent should accompany a net depression of the oceanic side of Earth, which would lower sea level. Note that supercontinents are likely to be surrounded by subduction zones during their lifetime, and a fully developed downwelling system within the oceanic side of Earth is not necessarily expected (Zhong et al., 2007). However, such a downwelling system is not necessarily required: we have inferred a net depression of the oceanic seafloor because net uplift must have occurred on the supercontinent. Therefore, uplifted seafloor on the oceanic side simply becomes less uplifted during the lifetime of a supercontinent, which would drop sea level.

This analysis suggests a cycle of net sea-level drop during the supercontinent phase of the Wilson cycle caused by a net decrease in dynamic topography in oceanic areas (e.g., Fig. 1, mode 1), followed by sea-level rise during the dispersal and reaggregation phases caused by net continental motion away from the uplifted center of a supercontinent (Fig. 1, mode 2). This pattern largely follows the gross pattern of sea-level trends: a period of sea-level fall (ca. 450 to ca. 250 Ma) (Cogné and Humler, 2008) occurred approximately during Pangean stability (ca. 400 and ca. 200 Ma) (Collins, 2003) followed by a period of sea-level rise during continental breakup (ca. 200 and ca. 100 Ma) (Cogné and Humler, 2008). Of course, dynamic topography is only one of several factors that affect sea level, so we do not expect a pure correlation between sea level and the Wilson cycle. For example, changes in the volume of the mid-ocean-ridge system are thought to be responsible for some of the most recent 100–200 m drop in sea level during the past ~100 Ma (e.g., Xu et al., 2006; Müller et al., 2008), which occurred during a period of continental dispersal. Furthermore, the complexity and time-dependence of mantle flow will produce aspects of flow that may not be directly associated with the Wilson cycle, such as the growing upwelling beneath the Pacific basin (Fig. 2A), which is currently responsible for much of the present-day predicted sea-level rise (Fig. 5B). Nevertheless, we anticipate that dynamic topography may be responsible for up to ~100 m of sea-level rise during times of supercontinent dispersal and reaggregation (as is presently observed) and a similar

amount of sea-level drop during times of supercontinent stability. Thus, the effect of dynamic topography on sea-level change should be comparable in magnitude to other major causes of sea-level rise or fall.

CONCLUSIONS

We have estimated that sea level is currently higher by ~90 ± 20 m due to the convective dynamics of the mantle interior. This time-dependent deflection of the seafloor by dynamic topography is presently causing sea level to rise at rates that may be as high as 1.0 m/Ma. Much of the associated uncertainty is due to the poorly constrained mantle viscosity structure, but it is also due to the difficulty of constraining the time-dependence of downwelling mantle flow. Because mantle downwelling causes dense slabs to fall away from Earth's surface, the dynamic topography they induce at that surface will get smaller with time. Unless global mantle flow models can accurately reinject slabs into the upper mantle at subduction zones, such models cannot reliably constrain the influence of mantle downwelling on sea-level change. At present, time-dependent treatment of subduction zones is more accurately realized in idealized (e.g., Gurnis, 1990) or analytic (Husson and Conrad, 2006) models, which should produce better constraints on downwelling-induced sea-level change compared to advection-dominated models of global mantle flow such as this study or Moucha et al. (2008).

The motion of the continents over Earth's dynamic topography can cause between 0.3 m/Ma of sea-level rise and 0.3 m/Ma of sea-level fall, depending on the net motion of the lithosphere relative to the deep mantle. Together with a net positive contribution of up to 1 m/Ma from growing mantle upwellings, our estimates suggest a wide range of sea-level rise contributions, but they do indicate that dynamic topography is probably currently producing net sea-level rise with a median value of ~0.5 m/Ma. This rate is significantly smaller than the rate implied by the 100 m of rise in 30 Ma (3.3 m/Ma) estimated by Moucha et al. (2008). We note, however, that Moucha et al.'s (2008) study included significant (~2 km) dynamic topography near mid-ocean ridges, which may be associated with low-velocity anomalies that have been imaged tomographically beneath ridges above 200 km depth (e.g., Ritsema et al., 2004). We do not include these features in our model because near-surface mantle anomalies will be strongly affected by both thermal diffusion and the details of the plate boundary implementation, both of which are difficult to implement in a time-dependent, backward-advection model (e.g., Conrad and Gurnis, 2003). Nevertheless, many of the dynamic topography trends predicted here (e.g., Fig. 3) are similar to those predicted by Moucha et al. (2008), who also showed large areas of the Pacific and circum-African ocean basins becoming shallower with time.

We have argued that a combination of continental motion and dynamic seafloor uplift should sustain as much as ~1 m/Ma of sea-level rise during the ongoing continental dispersal phase of the Wilson cycle. When included within a global tally of estimates for the various Cenozoic sea-level change mechanisms (Fig. 6), the dynamic topography contribution (~65 m rise) is comparable in magnitude to the net sea-level drop due to ice-sheet formation (~50 m; Harrison, 1990) or ocean area increase due to the India-Asia collision (~25 m; Harrison, 1990). It is also comparable to the uncertain rise that may be associated with the increased sedimentation and seafloor volcanism that are associated with increasing seafloor age (~60 and ~20 m, respectively; Müller et al., 2008; Harrison, 1990). Only ridge volume changes, estimated at 125–250 m by Xu et al. (2006) and ~200 m by Müller et al. (2008), are significantly more important as a Cenozoic source (Fig. 6). As a result, the introduction of a persistent dynamic topography-induced sea-level rise to the global tally (Fig. 6) produces a predicted Cenozoic sea-level change (140 m) that lies approximately midway between the curves presented in Haq et al. (1987) and Miller et al. (2005), which estimate sea-level drops of 240 m and 50 m, respectively. Previous studies (e.g., Müller et al., 2008; Spasojeviç et al., 2008) have inferred that some of the discrepancy between these curves is associated with subsidence of the U.S. east coast, where the measurements by Miller et al. (2005) were made. Our study suggests that as much as 1 m/Ma of eustatic sea-level rise is caused by the time-dependent nature of dynamic topography, and it should be included in attempts to match observations of long-term sea-level change to tallies of the various sources of that change.

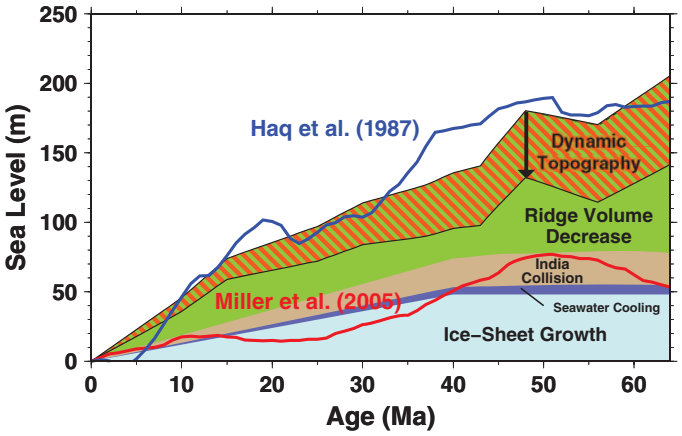

Figure 6. Variation of Cenozoic sea level, as inferred by Miller et al. (2005) (red line) and by Haq et al. (1987) (blue line), and the relative amplitudes of the different possible sources of this sea-level change. The effects of ice-sheet growth (light blue), seawater cooling (dark blue), and continental area shrinkage resulting from India-Asia collision (brown) are estimated from Harrison (1990). The effect of ridge volume decrease is estimated using the Hall (2002) case of Xu et al. (2006), and it is shown in green. Finally, the possible effect of dynamic topography is shown in red hatches, and produces sea-level rise of up to 1 m/Ma, based on the estimates determined here.

ACKNOWLEDGMENTS

This work was supported by National Science Foundation (NSF) grant EAR-0914712 (to Conrad). We thank S. Zhong and another anonymous referee for critical reviews that greatly improved the manuscript, and C. Lithgow-Bertelloni for helpful discussions and comments.

REFERENCES CITED

Becker, T.W., 2006, On the effect of temperature and strain-rate dependent viscosity on global mantle flow, net rotation, and plate-driving forces: Geophysical Journal International, v. 167, p. 943–957, doi: 10.1111/j.1365-246X.2006.03172.x.

Becker, T.W., 2008, Azimuthal seismic anisotropy constrains net rotation of the lithosphere: Geophysical Research Letters, v. 35, p. L05303, doi: 10.1029/2007GL032928.

Bokelmann, G.H.R., 2002, Which forces drive North America?: Geology, v. 30, p. 1027–1030, doi: 10.1130/0091-7613(2002)030<1027:WFDNA>2.0.CO;2.

Bond, G.C., 1976, Evidence for continental subsidence in North America during the Late Cretaceous global submergence: Geology, v. 4, p. 557–560, doi: 10.1130/0091-7613(1976)4<557:EFCSIN>2.0.CO;2.

Bunge, H.-P., and Grand, S.P., 2000, Mesozoic plate-motion history below the northeast Pacific Ocean from seismic images of the subducted Farallon slab: Nature, v. 405, p. 337–340, doi: 10.1038/35012586.

Cadek, O., and Fleitout, L., 2003, Effect of lateral viscosity variations in the top 300 km on the geoid and dynamic topography: Geophysical Journal International, v. 152, p. 566–580, doi: 10.1046/j.1365-246X.2003.01859.x.

Cogné, J.-P., and Humler, E., 2008, Global scale patterns of continental fragmentation: Wilson's cycles as a constraint for long-term sea-level changes: Earth and Planetary Science Letters, v. 273, p. 251–259, doi: 10.1016/j.epsl.2008.06.030.

Cogné, J.-P., Humler, E., and Courtillot, V., 2006, Mean age of oceanic lithosphere drives eustatic sea-level change since Pangea breakup: Earth and Planetary Science Letters, v. 245, p. 115–122, doi: 10.1016/j.epsl.2006.03.020.

Colin, P., and Fleitout, L., 1990, Topography of the ocean floor: Thermal evolution of the lithosphere and interaction of deep mantle heterogeneities with the lithosphere: Geophysical Research Letters, v. 17, p. 1961–1964, doi: 10.1029/GL017i011p01961.

Collins, W.J., 2003, Slab pull, mantle convection, and Pangaean assembly and dispersal: Earth and Planetary Science Letters, v. 205, p. 225–237, doi: 10.1016/S0012-821X(02)01043-9.

Conrad, C.P., and Gurnis, M., 2003, Mantle flow, seismic tomography and the breakup of Gondwanaland: Integrating mantle convection backwards in time: Geochemistry, Geophysics, Geosystems, v. 4, p. 1031, doi: 10.1029/2001GC000299.

Conrad, C.P., and Lithgow-Bertelloni, C., 2006, Influence of continental roots and asthenosphere on plate-mantle coupling: Geophysical Research Letters, v. 33, p. L05312, doi: 10.1029/2005GL025621.

Conrad, C.P., Lithgow-Bertelloni, C., and Louden, K.E., 2004, Iceland, the Farallon slab, and dynamic topography of the North Atlantic: Geology, v. 32, p. 177–180, doi: 10.1130/G20137.1.

Conrad, C.P., Behn, M.D., and Silver, P.G., 2007, Global mantle flow and the development of seismic anisotropy: Differences between the oceanic and continental upper mantle: Journal of Geophysical Research, v. 112, p. B07317, doi: 10.1029/2006JB004608.

DeMets, C., Gordon, R.G., Argus, D.F., and Stein, S., 1994, Effect of recent revisions to the geomagnetic reversal time scale on estimates of current plate motions: Geophysical Research Letters, v. 21, p. 2191–2194, doi: 10.1029/94GL02118.

Gripp, A.E., and Gordon, R.G., 2002, Young tracks of hotspots and current plate velocities: Geophysical Journal International, v. 150, p. 321–361, doi: 10.1046/j.1365-246X.2002.01627.x.

Gurnis, M., 1988, Large-scale mantle convection and the aggregation and dispersal of supercontinents: Nature, v. 332, p. 695–699, doi: 10.1038/332695a0.

Gurnis, M., 1990, Ridge spreading, subduction, and sea-level fluctuations: Science, v. 250, p. 970–972, doi: 10.1126/science.250.4983.970.

Gurnis, M., 1993, Phanerozoic marine inundation of continents driven by dynamic topography above subducting slabs: Nature, v. 364, p. 589–593, doi: 10.1038/364589a0.

Gurnis, M., Mitrovica, J.X., Ritsema, J.E., and van Heijst, H.-J., 2000, Constraining mantle density structure using geological evidence of surface uplift rates: The case of the African Superplume: Geochemistry, Geophysics, Geosystems, v. 1, 1999GC000035, doi: 10.1029/1999GC000035.

Hager, B.H., 1984, Subducted slabs and the geoid: Constraints on mantle rheology and flow: Journal of Geophysical Research, v. 89, p. 6003–6015, doi: 10.1029/JB089iB07p06003.

Hager, B.H., Clayton, R.W., Richards, M.A., Comer, R.P., and Dziewonski, A.M., 1985, Lower mantle heterogeneity, dynamic topography and the geoid: Nature, v. 313, p. 541–545, doi: 10.1038/313541a0.

Hall, R., and Spakman, W., 2002, Subducted slabs beneath the eastern Indonesia–Tonga region: insights from tomography: Earth and Planetary Science Letters, v. 201, p. 321–336, doi: 10.1016/S0012-821X(02)00705-7.

Harrison, C.G.A., 1990, Long-term eustasy and epeirogeny in continents, *in* Revelle, R.R., ed., Sea-Level Change: Washington, D.C., National Academy Press, p. 141–158.

Haq, B.U., Hardenbol, J., and Vail, P.R., 1987, Chronology of fluctuating sea levels since the Triassic: Science, v. 235, p. 1156–1167, doi: 10.1126/science.235.4793.1156.

Heine, C., Müller, R.D., Steinberger, B., and Torsvik, T.H., 2008, Subsidence in intracontinental basins due to dynamic topography: Physics of the Earth and Planetary Interiors, v. 171, p. 252–264, doi: 10.1016/j.pepi.2008.05.008.

Hernlund, J.W., Tackley, P.J., and Stevenson, D.J., 2008, Buoyant melting instabilities beneath extending lithosphere: 1. Numerical models: Journal of Geophysical Research, v. 113, B04405, doi: 10.1029/2006JB004862.

Hoffman, P.F., 1991, Did the breakout of Laurentia turn Gondwanaland inside-out?: Science, v. 252, p. 1409–1412, doi: 10.1126/science.252.5011.1409.

Husson, L., 2006, Dynamic topography above retreating subduction zones: Geology, v. 34, p. 741–744, doi: 10.1130/G22436.1.

Husson, L., and Conrad, C.P., 2006, Tectonic velocities, dynamic topography, and relative sea level: Geophysical Research Letters, v. 33, L18303, doi: 10.1029/2006GL026834.

Husson, L., Conrad, C.P., and Faccenna, C., 2008, Tethyan closure, Andean orogeny, and westward drift of the Pacific basin: Earth and Planetary Science Letters, v. 271, p. 303–310, doi: 10.1016/j.epsl.2008.04.022.

Jordan, T.H., 1975, The continental tectosphere: Reviews of Geophysics, v. 13, p. 1–12, doi: 10.1029/RG013i003p00001.

Karato, S.-I., and Karki, B.B., 2001, Origin of lateral variation of seismic wave velocities and density in the deep mantle: Journal of Geophysical Research, v. 106, p. 21,771–21,783, doi: 10.1029/2001JB000214.

Kominz, M.A., 1984, Oceanic ridge volumes and sea level change—An error analysis, *in* Schlee, J., ed., Interregional Unconformities and Hydrocarbon Accumulation: American Association of Petroleum Geologists Memoir 36, p. 109–127.

Le Stunff, Y., and Ricard, Y., 1997, Partial advection of equidensity surfaces: A solution for the dynamic topography problem?: Journal of Geophysical Research, v. 102, p. 24,655–24,667, doi: 10.1029/97JB02346.

Lithgow-Bertelloni, C., and Gurnis, M., 1997, Cenozoic subsidence and uplift of continents from time-varying dynamic topography: Geology, v. 25, p. 735–738, doi: 10.1130/0091-7613(1997)025<0735:CSAUOC>2.3.CO;2.

Lithgow-Bertelloni, C., and Richards, M.A., 1998, The dynamics of Cenozoic and Mesozoic plate motions: Reviews of Geophysics, v. 36, p. 27–78, doi: 10.1029/97RG02282.

Lithgow-Bertelloni, C., and Silver, P.G., 1998, Dynamic topography, plate-driving forces and the African superswell: Nature, v. 395, p. 269–272, doi: 10.1038/26212.

Liu, L., Spasojeviç, S., and Gurnis, M., 2008, Reconstructing Farallon plate subduction beneath North America back to the Cretaceous: Science, v. 322, p. 934–938, doi: 10.1126/science.1162921.

Lowman, J.P., and Jarvis, G.T., 1999, Effects of mantle heat source distribution on supercontinent stability: Journal of Geophysical Research, v. 104, p. 12,733–12,746, doi: 10.1029/1999JB900108.

Masters, G., Laske, G., Bolton, H., and Dziewonski, A., 2000, The relative behavior of shear velocity, bulk sound speed, and compressional velocity in the mantle: Implications for chemical and thermal structure, *in* Karato, S.-I., Forte, A.M., Liebermann, R.C., Masters, G., and Stixrude, L., eds., Earth's Deep Interior. Mineral Physics and Tomography from the Atomic to the Global Scale: American Geophysical Union (AGU) Monograph Series, Seismology and Mineral Physics, v. 117, p. 63–87.

Miller, K.G., Kominz, M.A., Browning, J.V., Wright, J.D., Mountain, G.S., Katz, M.E., Sugarman, P.J., Cramer, B.S., Christie-Blick, N., and Pekar, S.F., 2005, The Phanerozoic record of global sea-level change: Science, v. 310, p. 1293–1298, doi: 10.1126/science.1116412.

Mitrovica, J.X., 1996, Haskell (1935) revisited: Journal of Geophysical Research, v. 101, p. 555–569, doi: 10.1029/95JB03208.

Mitrovica, J.X., Beaumont, C., and Jarvis, G.T., 1989, Tilting of continental interiors by the dynamical effects of subduction: Tectonics, v. 8, p. 1079–1094, doi: 10.1029/TC008i005p01079.

Moucha, R., Forte, A.M., Mitrovica, J.X., and Daradich, A., 2007, Geodynamic implications of lateral variations in mantle rheology on convection related observables and inferred viscosity models: Geophysical Journal International, v. 169, p. 113–135, doi: 10.1111/j.1365-246X.2006.03225.x.

Moucha, R., Forte, A.M., Mitrovica, J.X., Rowley, D.B., Quere, S., Simons, N.A., and Grand, S.P., 2008, Dynamic topography and long-term sea-level variations: There is no such thing as a stable continental platform: Earth and Planetary Science Letters, v. 271, p. 101–108, doi: 10.1016/j.epsl.2008.03.056.

Müller, R.D., Sdrolias, M., Gaina, C., Steinberger, B., and Heine, C., 2008, Long-term sea-level fluctuations driven by ocean basin dynamics: Science, v. 319, p. 1357–1362, doi: 10.1126/science.1151540.

Paulson, A., Zhong, S., and Wahr, J., 2005, Modelling post-glacial rebound with lateral viscosity variations: Geophysical Journal International, v. 163, p. 357–371, doi: 10.1111/j.1365-246X.2005.02645.x.

Paulson, A., Zhong, S., and Wahr, J., 2007, Inference of mantle viscosity from GRACE and relative sea level data: Geophysical Journal International, v. 171, p. 497–508.

Phillips, B.R., and Bunge, H.P., 2005, Heterogeneity and time dependence in 3D spherical mantle convection models with continental drift: Earth and Planetary Science Letters, v. 233, p. 121–135, doi: 10.1016/j.epsl.2005.01.041.

Pitman, W.C., 1978, Relationship between eustasy and stratigraphic sequences of passive margins: Geological Society of America Bulletin, v. 89, p. 1389–1403, doi: 10.1130/0016-7606(1978)89<1389:RBEASS>2.0.CO;2.

Ritsema, J., van Heijst, H.J., and Woodhouse, J.H., 2004, Global transition zone tomography: Journal of Geophysical Research, v. 109, B02302, doi: 10.1029/2003JB002610.

Sdrolias, M., and Müller, R.D., 2006, Controls on back-arc basin formation: Geochemistry, Geophysics, Geosystems, v. 7, Q04016, doi: 10.1029/2005GC001090.

Spasojeviç, S., Liu, L., Gurnis, M., and Müller, R.D., 2008, The case for dynamic subsidence of the U.S. east coast, since the Eocene: Geophysical Research Letters, v. 35, L08305, doi: 10.1029/2008GL033511.

Tan, E., Choi, E., Thoutireddy, P., Gurnis, M., and Aivazis, M., 2006, GeoFramework: Coupling multiple models of mantle convection within a computational framework: Geochemistry, Geophysics, Geosystems, v. 7, Q06001, doi: 10.1029/2005GC001155.

Thoraval, C., and Richards, M.A., 1997, The geoid constraint in global geodynamics: Viscosity structure, mantle heterogeneity models and boundary conditions: Geophysical Journal International, v. 131, p. 1–8, doi: 10.1111/j.1365-246X.1997.tb00591.x.

Torsvik, T.H., Müller, R.D., Van der Voo, R., Steinberger, B., and Gaina, C., 2008, Global plate motion frames: Toward a unified model: Reviews of Geophysics, v. 46, RG3004, doi: 10.1029/2007RG000227.

van der Hilst, R., 1995, Complex morphology of subducted lithosphere in the mantle beneath the Tonga Trench: Nature, v. 374, p. 154–157, doi: 10.1038/374154a0.

Wilson, J.T., 1966, Did the Atlantic close and then re-open?: Nature, v. 211, p. 676–681, doi: 10.1038/211676a0.

Xu, X., Lithgow-Bertelloni, C., and Conrad, C.P., 2006, Global reconstructions of Cenozoic seafloor ages: Implications for bathymetry and sea level: Earth and Planetary Science Letters, v. 243, p. 552–564, doi: 10.1016/j.epsl.2006.01.010.

Zhong, S., and Davies, G.F., 1999, Effects of plate and slab viscosities on geoid: Earth and Planetary Science Letters, v. 170, p. 487–496, doi: 10.1016/S0012-821X(99)00124-7.

Zhong, S., Zuber, M.T., Moresi, L., and Gurnis, M., 2000, Role of temperature-dependent viscosity and surface plates in spherical shell models of mantle convection: Journal of Geophysical Research, v. 105, p. 11,063–11,082, doi: 10.1029/2000JB900003.

Zhong, S., Zhang, N., Li, Z.-X., and Roberts, J.H., 2007, Supercontinent cycles, true polar wander, and very long-wavelength mantle convection: Earth and Planetary Science Letters, v. 261, p. 551–564, doi: 10.1016/j.epsl.2007.07.049.

Zhong, S., McNamara, A., Tan, E., Moresi, L., and Gurnis, M., 2008, A benchmark study on mantle convection in a 3-D spherical shell using CitcomS: Geochemistry, Geophysics, Geosystems, v. 9, Q10017, doi: 10.1029/2008GC002048.

MANUSCRIPT RECEIVED 11 NOVEMBER 2008
REVISED MANUSCRIPT RECEIVED 23 FEBRUARY 2009
MANUSCRIPT ACCEPTED 27 FEBRUARY 2009

Printed in the USA